Earthquakes and Structures, *Vol. 9, No. 5 (2015) 957-981*
DOI: http://dx.doi.org/10.12989/eas.2015.9.5.957

Numerical modeling and analysis of RC frames subjected to multiple earthquakes

Adel E. Abdelnaby*[1] and Amr S. Elnashai[2a]

[1]*Department of Civil Engineering, University of Memphis, 3815 Central Ave, Memphis, TN 38152, USA*
[2]*Department of Civil and Environmental Engineering, University of Illinois at Urbana-Champaign, 205 N, Mathews Ave, Urbana, IL 61801, USA*

(Received June 16, 2014, Revised July 13, 2015, Accepted July 13, 2015)

Abstract. Earthquakes occur as a cluster in many regions around the world where complex fault systems exist. The repeated shaking usually induces accumulative damage to affected structures. Damage accumulation in structural systems increases their level of degradation in stiffness and also reduces their strength. Many existing analytical tools of modeling RC structures lack the salient damage features that account for stiffness and strength degradation resulting from repeated earthquake loading. Therefore, these tools are inadequate to study the response of structures in regions prone to multiple earthquakes hazard. The objective of this paper is twofold: (a) develop a tool that contains appropriate damage features for the numerical analysis of RC structures subjected to more than one earthquake; and (b) conduct a parametric study that investigates the effects of multiple earthquakes on the response of RC moment resisting frame systems. For this purpose, macroscopic constitutive models of concrete and steel materials that contain the aforementioned damage features and are capable of accurately capturing materials degrading behavior, are selected and implemented into fiber-based finite element software. Furthermore, finite element models that utilize the implemented concrete and steel stress-strain hysteresis are developed. The models are then subjected to selected sets of earthquake sequences. The results presented in this study clearly indicate that the response of degrading structural systems is appreciably influenced by strong-motion sequences in a manner that cannot be predicted from simple analysis. It also confirms that the effects of multiple earthquakes on earthquake safety can be very considerable.

Keywords: RC frames; multiple earthquakes; damage accumulation; stiffness and strength degradation

1. Introduction

RC structures are vulnerable to multiple earthquake excitations. In post-earthquake field investigations, extensive damage of RC buildings and bridges subjected to more than one earthquake was reported. In many cases the failure of these structures was due to the loss of stiffness and strength of structural components as a result of damage accumulation induced by repeated shaking. This was observed in structures that remained intact after a large main-shock and

*Corresponding author, Professor, E-mail: bdelnaby@memphis.edu
[a]Ph.D., E-mail: aelnash@illinois.edu

 ISSN: 2092-7614 (Print), 2092-7622 (Online)

collapsed a few days later in a smaller aftershock. Fig. 1 illustrates the extent of damage and collapse of a building second story during the main- and after-shock of the M_w 7.3 Gediz earthquake in March 28, 1970, in Turkey. Failure of structures in a similar manner has been also reported in recent earthquake sequences including the Umbria-Marche (Italy 1997), Kocaeli and Duzce (Turkey 1999), Chile (2012), Christchurch (New Zealand 2011 and 2012) and Tohoku (Japan 2011 and 2012) earthquakes as indicated in Abdelnaby (2012).

Extensive research has been conducted on the seismic vulnerability of buildings and lifeline systems. Previous research focused mainly on the response of structures subjected to one (the most damaging) earthquake, and therefore neglected the effects of prior shaking on the dynamic characteristics and strength of the damaged structural systems. In addition, existing seismic design and evaluation procedures assume that structures remain in their initially undamaged condition while experiencing seismic demands at different performance levels.

Limited research has addressed the effects of multiple earthquakes on the seismic behavior of structures including RC and steel buildings and bridges (Mahin 1980, Aschheim *et al*. 1999, Amadio *et al*. 2003, Fragiacomo *et al*. 2004, Li and Ellingwood 2007, Hatzigeorgiou *et al*. 2009, 2010a, b, Raghunandan *et al*. 2012, Ghosh *et al*. 2013). Single Degree of Freedom (SDOF) systems (or system level based models) incorporating different inelastic degrading hysteretic force-displacement relationships have been extensively used by many researchers such as Mahin (1980), Aschheim *et al*. (1999), Amadio *et al*. (2003), Hatzigeorgiou *et al*. (2009). Multi-Degree of Freedom (MDOF) systems such as moment resisting steel (Fragiacomo *et al*. 2004, Ellingwood *et al*. 2007, Ruiz-Garcia and Negrete-Manriquez 2011) and RC frames (Hatzigeorgiou *et al*. 2010, Raghunandan *et al*. 2012) are also studied.

(a) (b)

Fig. 1 Damaged building after the main-shock of Gediz earthquake in March 28, 1970 (a); the same building after a smaller aftershock (b) - after N.N. Ambraseys, private communication

Given the complexity of depicting the actual degrading behavior of structural systems, previous research utilized simplified methods to compensate for the absence of the important model features. In literature, simple numerical models are used including models of SDOF systems that incorporate a nonlinear force-displacement relationship as well as idealized models of MDOF frame systems which are based on the lumped plasticity modeling approach. Representing structures using simplified/idealized models leads to an inaccurate assessment of their response since many features are not precisely represented (Abdelnaby 2012). These features include, for SDOF systems, higher mode effects, localized failure behavior, and actions redistribution between structural components. In addition, the pre-specification of plastic hinge locations in the lumped plasticity approach used in MDOF systems does not capture localized deformations in terms of hinge length (or extent of inelasticity), yielding and buckling of steel, and crushing and cracking of concrete.

Table 1 Key aspects of previous studies of multiple earthquake effects on structures

Source	DOF	Structure Type	Model Idealization	Damage Features
Mahin 1980	SDOF	Oscillators	Bilinear force-displacement relationship	---
Aschheim *et al*. 1999	SDOF	Oscillators	Takeda force-displacement model (Takeda *et al*. 1970)	Stiffness and strength degradation as well as pinching
Amadio *et al*. 2003	SDOF	Oscillators	Different hysteresis assumptions	Stiffness and strength degradation as well as pinching
Fragiacomo *et al*. 2004	MDOF	Steel frames	Fiber-based FE model bilinear steel stress-strain relationship	---
Ellingwood *et al*. 2007	MDOF	Steel frames	Moment-rotation relationship at beam-column connections	Fracture of connection welds
Hatzigeorgiou *et al*. 2010	MDOF	RC frames	Bilinear moment-rotation relationship at beam-column connection	---
Ruiz-Garcia and Negrete-Manriquez 2011	MDOF	Steel frames	Fiber-based FE model bilinear steel stress-strain relationship	Strength degradation due to beam fracture
Raghunandan *et al*. 2012	MDOF	RC frames	Nonlinear moment-rotation relationship at beam-column connections	Strength degradation due to repeated loading
Ghosh *et al*. 2013	SDOF	Bridge pier	Single column section modeled using a nonlinear fiber section with distributed plasticity	Strength degradation
This study	MDOF	RC frames	Fiber-based FE model Energy based plastic damage concrete model Steel model based on the modified Menegotto-Pinto constitutive model	Stiffness and strength degradation in concrete Buckling and fracture of steel bars

In this study, a near-fully realistic assessment of the demands upon and performance of degrading RC structures subjected to repeated seismic loadings is aimed. Distributed plasticity models of RC structures, as opposed to SDOF and lumped plasticity MDOF models are developed and used. The models contain essential damage features at steel and concrete materials level and that including stiffness and strength degradation alongside with pinching of stress-strain loops. A summary of the key aspects of previous studies are provided in Table 1. These aspects include the number of studied degrees of freedom, as well as damage features employment at the material, component, and system levels. The details of this study are contrasted to the studies surveyed in the literature as highlighted in Table 1. This serves to highlight the level of complexity and realism achieved in this paper that was not achieved elsewhere.

2. Constitutive material models

Development of a tool that models the important damage features essential to study the degrading behavior of RC structures prone to multiple earthquakes is sought in this study. In order to accurately capture the behavior at the material level, damage features are represented in the stress-strain hysteresis (at each section fiber). This is done in contrary to prior studies that used the previously discussed simplified approaches.

Steel and concrete constitutive models that account for damage accumulation in terms of stiffness and strength degradation as well as pinching are introduced and the implementation process in fiber-based finite element software is discussed. The damage features in the steel model include Bauschinger effects, buckling of reinforcement bars, and fracture. The concrete constitutive stress-strain relationship is based on fiber-energy-based damage model and stiffness degradation in continuum damage mechanics. More detail on the steel and concrete constitutive relationships is discussed in Abdelnaby (2012).

2.1 Steel model

The stress-strain relationship of reinforcing bars steel material is based on the modified Guiffre'-Menegotto-Pinto relationship (Menegotto and Pinto 1973, Gomes and Appleton 1997). The steel model simulates the following characteristics, which are shown in Fig. 2: (1) elastic, yielding and hardening branching in the first excursion; (2) Bauschinger effect which consists of (a) reduction of the yield stress after a reverse which increases with the enlargement of the plastic strain component of the last excursion, (b) decrease of the curvature in the transition zone between the elastic and plastic branches; (3) inelastic buckling of reinforcing bars after crushing of bar confining concrete; and (4) Fracture of steel under strains higher than the material rupture strain is represented in the constitutive model by the complete loss of stiffness and strength of reinforcing steel.

Under large load excursions and post-crushing of the RC section concrete cover, confinement of compression bars from buckling is lost (Fig. 3). In this study, the buckling stress-strain path is simulated by a simplified model based on the equilibrium of a plastic mechanism of the buckled bar, as shown in Fig. 4. The buckling stress-strain relationship is a function of bar diameter, yield strength of steel, spacing between transverse reinforcement (ties or stirrups), axial stress applied on the bar, as well as the crushing strain of surrounding concrete (since buckling is not initiated unless the cover concrete reaches its crushing strain). Table 2 lists the parameters that are needed

for steel model definition.

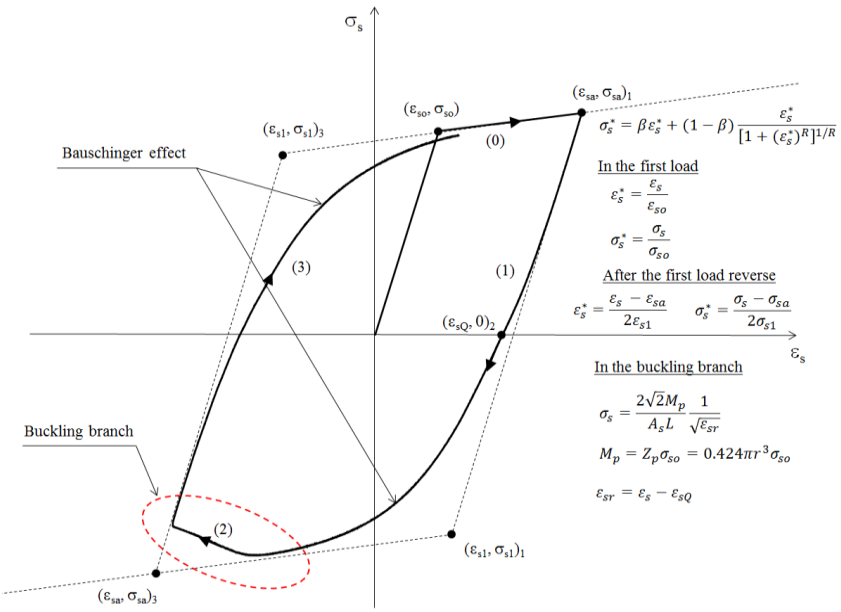

Fig. 2 Characteristics of steel stress-strain relationship including bar buckling (Gomes *et al*. 1997)

Fig. 3 Buckled reinforcing bars of a reinforced concrete column after Chile earthquake

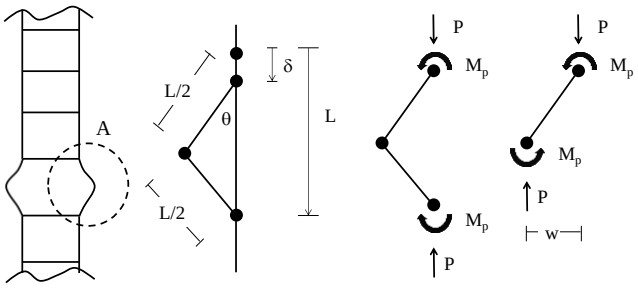

Fig. 4 Equilibrium of buckled longitudinal steel bar

Table 2 Parameters of the cyclic steel constitutive model

Parameter	Definition	Notes
ε_s	Absolute strain	
σ_s	Absolute stress	
β	E_{s1}/E_s	Ratio between hardening stiffness and tangent modulus of elasticity
E_{s1}	Hardening stiffness	
E_s	Tangent modulus of elasticity	
R	$R_o - \frac{\alpha_1 \xi}{\alpha_2 + \xi}$	The distance of elastic curve, which simulates the Bauschinger effect
α_1	Material constant	
α_2	Material constant	
ξ	Absolute plastic strain of the last excursion	
ε_s^*	$\frac{\varepsilon_s}{\varepsilon_{so}}$	Parameters defining the steel model in the first load, branch (0) in Fig. 2
σ_s^*	$\frac{\sigma_s}{\sigma_{so}}$	
ε_{so}	Strain at yield point of bilinear envelope	
σ_{so}	Stress at yield point of bilinear envelope	
ε_s^*	$\frac{\varepsilon_s - \varepsilon_{sa}}{2\varepsilon_{sa}}$	Parameters defining the steel model after the first reverse, branches (1) & (3) in Fig. 2
σ_s^*	$\frac{\sigma_s - \sigma_{sa}}{2\sigma_{sa}}$	
ε_{sa}	Strain at inversion points (Fig. 2)	
σ_{sa}	Stress at inversion points (Fig. 2)	
M_p	Plastic moment of the bar of a circular section	
Z_p	Plastic modulus of the bar section	
r	Bar radius	
L	Spacing between stirrups/ties	Parameters defining the steel model in buckling, branch (2) Fig. 2
A_s	Cross sectional area of the bar	
ε_{sr}	$\varepsilon_s - \varepsilon_{sQ}$	
ε_{sQ}	Strain at zero stress at load sign reversal (from tension to compression) as shown in Fig. 2	

2.2 Concrete model

The concrete model utilized in this study is developed using the concepts of fracture-energy-based damage and stiffness degradation in continuum damage mechanics (Lee and Fenves 1998). Two damage hardening variables are introduced to account for different damage states under

tensile (d_t) and compressive (d_c) stresses, as shown in Fig. 5. A simple degradation model is introduced to simulate the effect of damage on elastic stiffness and its recovery during crack opening and closure. Strength deterioration is modeled by using the effective stress (of cracked concrete) to control the evolution of the yield surface. The uniaxial stress-strain relationship of this model is developed by

$$\begin{gathered}\sigma_g = f_{go}\left[\left(1+a_g\right)\exp\left(-b_g\varepsilon^p\right) - a_g\exp\left(-2b_g\varepsilon^p\right)\right] \\ 1 - D_g = \exp\left(-d_g\varepsilon^p\right) \\ \overline{\sigma_g} = f_{go}\left[\left(1+a_g\right)\left(\exp\left(-b_g\varepsilon^p\right)\right)^{1-\left(\frac{d_g}{b_g}\right)} - a_g\left(\exp\left(-2b_g\varepsilon^p\right)\right)^{2-\left(\frac{d_g}{b_g}\right)}\right] \\ k_g = \frac{1}{g_g}\int_0^{\varepsilon^p}\sigma_g\left(\varepsilon^p\right)d\varepsilon^p\right) \\ g_g = \int_0^{\infty}\sigma_g\left(\varepsilon^p\right)d\varepsilon^p\right)\end{gathered} \tag{1}$$

where,

σ_g is the uniaxial stress

ε_p is the scalar plastic strain

f_{go} is the initial yield stress defined as the maximum stress without damage

a_g, b_g and d_g are constants

$\overline{\sigma_g}$ is the effective stress

3. Material model implementation

The material constitutive models for steel and concrete are implemented in the fiber-based analysis software Zeus-NL (Elnashai *et al*. 2010). Steel and concrete response was first examined under simple axial cyclic loading patterns and the behavior was verified by comparison with experimental data provided by Gomes *et al*. (1997), Lee and Fenves (1998). Optimization algorithms are developed and employed for faster convergence during expensive inelastic non-linear dynamic analyses. For further details regarding the material models implementation process, the reader is referred to Abdelnaby (2012).

3.1 Steel model

A simple reinforced concrete pier model is established, the pier characteristics in terms of concrete dimensions and steel reinforcement are shown in Fig. 6. Two modeling approaches are considered, the first approach uses the existing bi-linear steel stress-strain relationship (stl1) in Zeus-NL platform. The second approach utilizes the newly implemented steel model (stl4) that contains the appropriate damage features. The pier is subjected to lateral cyclic displacements and the load-displacement response for both cases is compared in Fig. 7. The comparison shows the gradual loss of stiffness and strength of the pier due to Bauschinger effects and buckling of

reinforcing bars as well as the sudden loss of strength resulting from steel fracture, for the stl4 case.

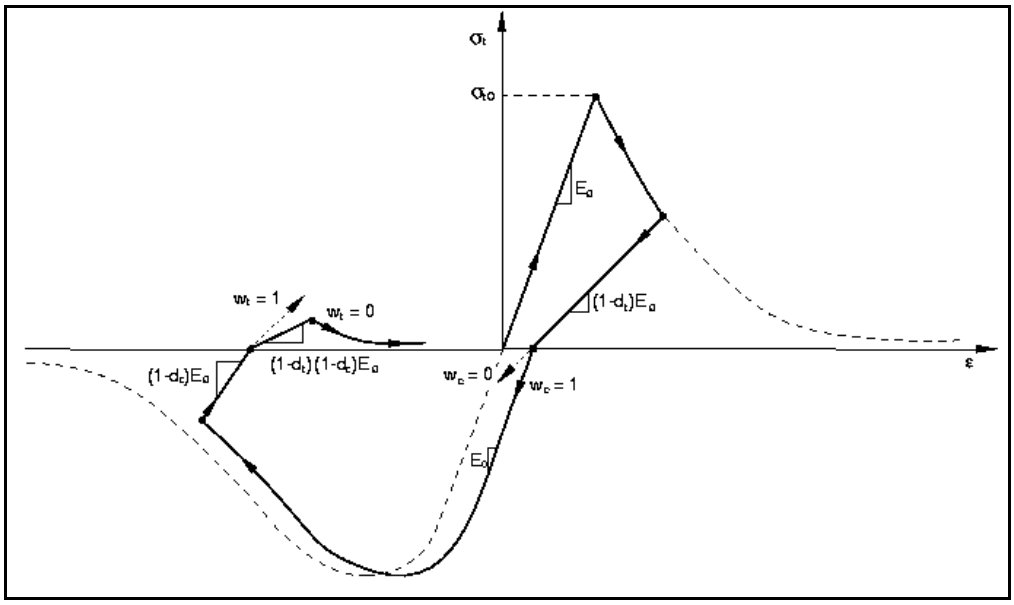

Fig. 5 Damage features of the concrete constitutive model (Lee and Fenves 1998)

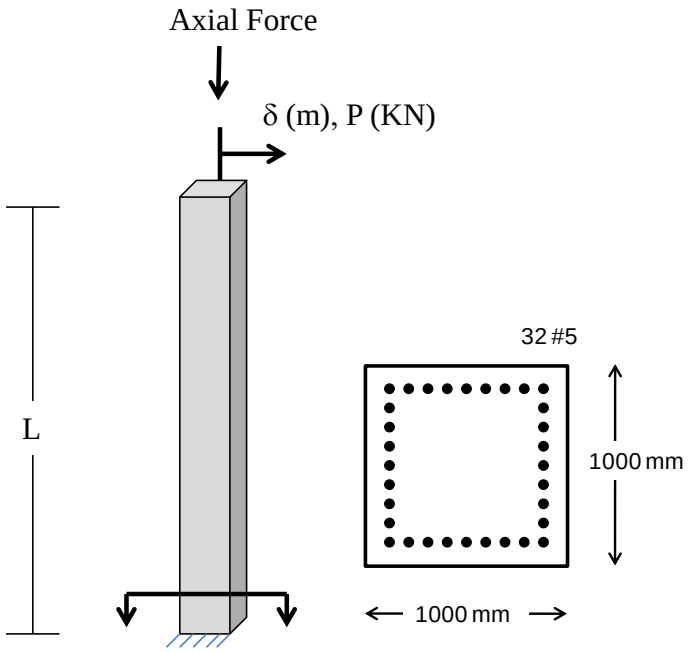

Fig. 6 Pier model, concrete dimensions and reinforcement

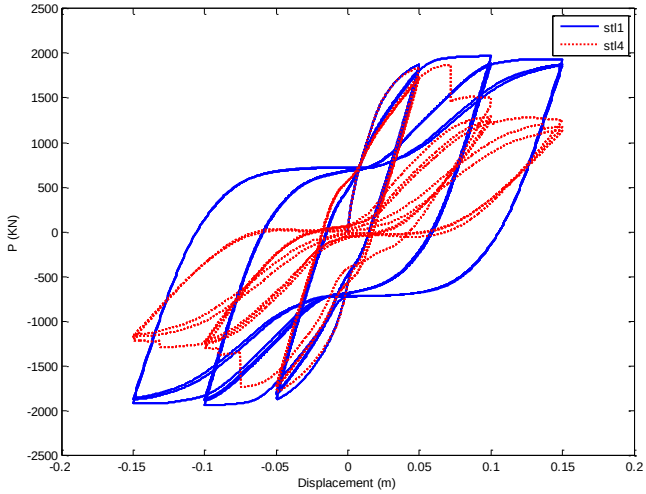

Fig. 7 Bauschinger, buckling, and fracture effects on the flexural hysteretic response of the pier model

3.2 Concrete model

Fig. 8 shows the uniaxial stress-strain response of the implemented concrete model (con5). The plot highlights the stiffness and strength degradation of the material response under simple axial cyclic, linearly increasing, sinusoidal strain loading. The stiffness degradation is obvious when the initial stiffness is compared with stiffnesses at high strain levels. Unlike other material models, a smooth transitional reduction of stiffness takes place in the model since the reduction of stiffness is based on a robust fracture-energy concept. The strength deterioration, in tension and compression, is captured as shown in Fig. 8. In addition, stiffness recovery (pinching effects) is depicted at the unloading curves where the stress state changes from tension to compression and vice versa.

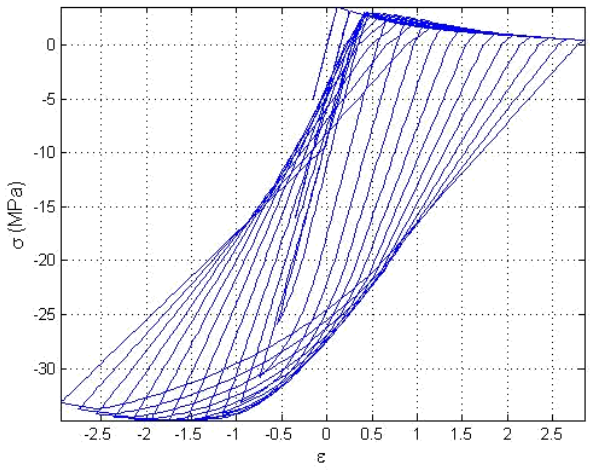

Fig. 8 Uniaxial cyclic behavior of implemented concrete model (con5)

4. Comparison between degrading and non-degrading predictions

An inelastic fiber-based finite element model is employed for a simple pier model using Zeus-NL platform. The cross sectional dimensions and reinforcement of the pier are shown in Fig. 6; the height of the pier is 4m and the spacing between stirrups is 250 mm. A mass is assigned at the top node of the pier model using the lumped (concentrated) mass element. The natural period of the pier is 0.46 seconds. Two modeling approaches are introduced, the first uses non-degrading concrete (Mander *et al*. 1988) and steel (bi-linear) models; while the second utilized the degrading material models discussed in the previous section.

The non-degrading and degrading pier models are subjected to two identical Loma Prieta earthquake ground motions applied in series. The displacement response of the undamaged (under one earthquake only) and damaged (under the second earthquake considering prior damage induced from the first earthquake) systems is plotted in Fig. 9. For the non-degrading system, the displacement response of the damaged and undamaged piers match very well after the piers reach their peak displacements. This observation was confirmed by Aschheim *et al*. (1999) when non-degrading simple degree of freedom models were used to study the effects of repeated earthquake on non-linear response of structures.

Prior to the peak displacement, the non-degrading displacement response shows longer period for the damaged system. While the post-peak displacement response matches very well for the first and second earthquakes. This is explained as follows: (1) the stiffness of the undamaged system at peak displacement reaches its lowest value and stays constant throughout the whole replicate motion analysis, since stiffness reduction in non-degrading models is influenced solely by the maximum displacement the system experiences; (2) P-Δ effects play a minimal role on stiffness reduction and that explains why the response after the peak displacement matched very well however the damaged systems experience residual displacements in some cases.

On the other hand, the response of degrading systems for the damaged and undamaged cases is quite different in terms of displacement amplitudes and predominant periods of vibration. The response of damaged and undamaged systems is discrepant pre- and post- the peak displacement, unlike the non-degrading case. In addition, longer periods are captured for the damaged systems as shown in Fig. 9.

5. Parametric analysis

5.1 Overview of frame models

The structure under consideration is a 3-story, 2-bay (longitudinal) and 4-bay (transverse) reinforced concrete frame, assumed to be located in Alisa Viejo, California (Fig. 10). The highlighted frame system in Fig. 10, in the transverse direction is of interest.

Three design concepts are introduced in this frame namely gravity, direct, and capacity design approaches. The building configuration and design procedures (design forces, sizing of beams and columns, and reinforcement detailing) as well as the finite element modeling of the frame systems using Zeus-NL are provided in Abdelnaby 2012.

Gravity load resisting frame is designed under the action of factored vertical dead and live loads only. Different loading configurations for live loads defined by the ASCE-07 code are used to maximize the design straining actions at critical sections. For the direct and capacity designed

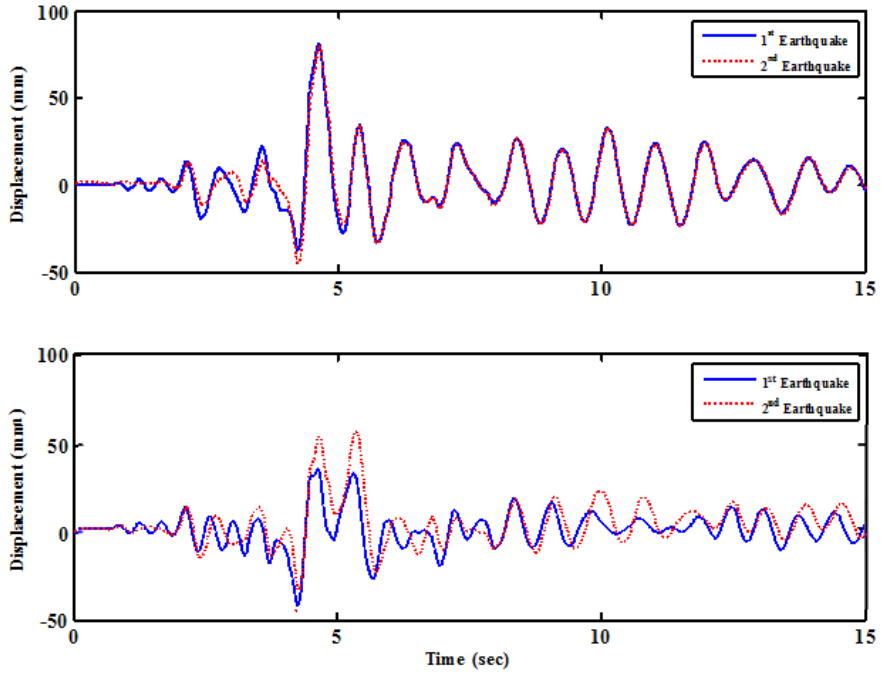

Fig. 9 Displacement response of undamaged and damaged piers under replicate motions using non-degrading (up) and degrading (down) material models

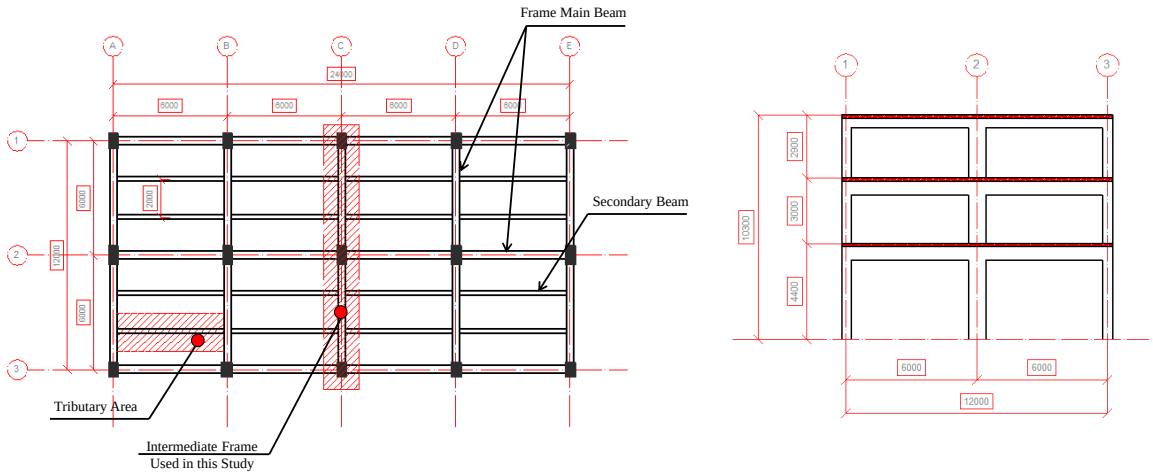

Fig. 10 Plan and elevation of the studied building

frames, seismic forces imposed on the systems are calculated based on ASCE-07 code, assuming the building is located in Aliso Vieji, California on type B soil (SDS=0.989 g and SD1=0.349 g). The direct designed frame is designed with accordance to the requirements of ACI 21.1.2 and ACI21.2 for ordinary moment frames. A response modification factor (R) equals 3 is used. The capacity designed frame satisfies ACI 21.5 and ACI 21.6 for beams and columns, for special

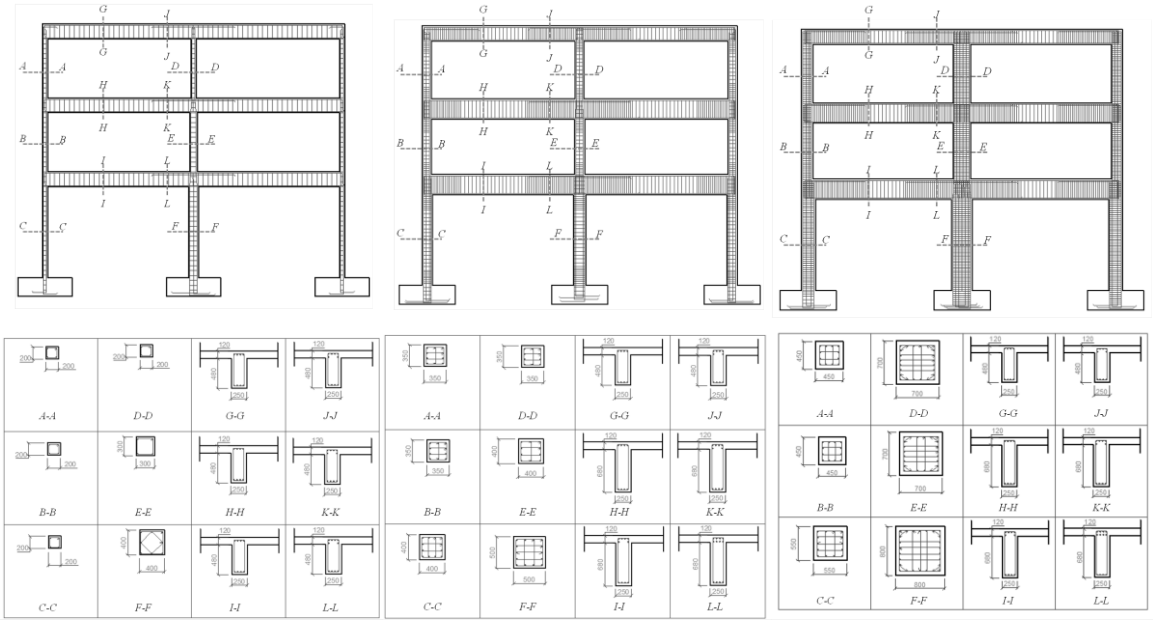

Fig. 11 Concrete dimensions and reinforcement for gravity (*left*), direct (*middle*) and capacity (*right*) designed frames (all longitudinal bars are # 7 and all stirrups are # 3 bars)

Table 3 First two natural periods of the frames

Frame ID	T_1	T_2
	(sec)	(sec)
Gravity	1.10	0.46
Direct	0.48	0.17
Capacity	0.28	0.09

moment frames (R=8). The equivalent static lateral load method is used to simplify the design procedure. Section sizes and reinforcement of the three frame systems are provided in Fig. 11.

Eigen value analyses are conducted to investigate the modes of vibration and fundamental periods of the frames. The first two natural periods of the structures are listed in the Table 3. The periods of vibration of the gravity designed frame are longer than the natural periods of the direct and capacity designed frames. This is because the gravity designed frame has lower initial stiffness than the direct and capacity design frames respectively. It is worth noting that the mode participation factor of the first mode exceeded 90% for the three frame systems.

In addition, conventional pushover analyses are carried out on the frame systems to determine their stiffness, strength and ductility (Table 4). Moreover, localized failures such as plastic hinging in beam and column elements are monitored (Fig. 12). The capacity designed frame exhibited the highest global stiffness, strength and displacement ductility. The direct designed frame has the lowest ductility while the gravity designed frame has the lowest stiffness and strength. Fig. 13 provides the capacity curves of the designed frame systems. It is noted that the pushover analysis is terminated at the first spalling of concrete or first fracture of steel reinforcing bars of any frame column.

The gravity designed frame exhibited plastic hinges at columns only while a soft first story behavior was observed in the direct designed frame. On the other hand, the capacity designed frame behaved as designed. Plastic hinges are formed first in beams, then action redistribution took place leading to localized failure in columns followed by collapse.

Table 4 Stiffness, strength and ductility of the frame systems

Frame ID	Stiffness	Strength	Ductility
	(KN/m)	KN	m/m
Gravity	93	179	4.80
Direct	670	680	3.93
Capacity	1670	1370	6.90

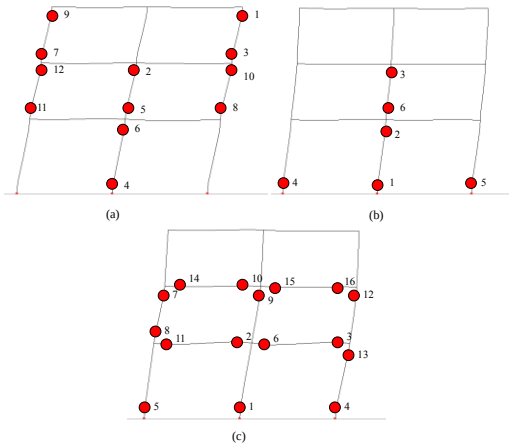

Fig. 12 Plastic hinges in frame systems, i.e., the numbers indicate the sequence of plastic hinges formation with respect to load steps; (a) gravity, (b) direct, (c) capacity designed frames

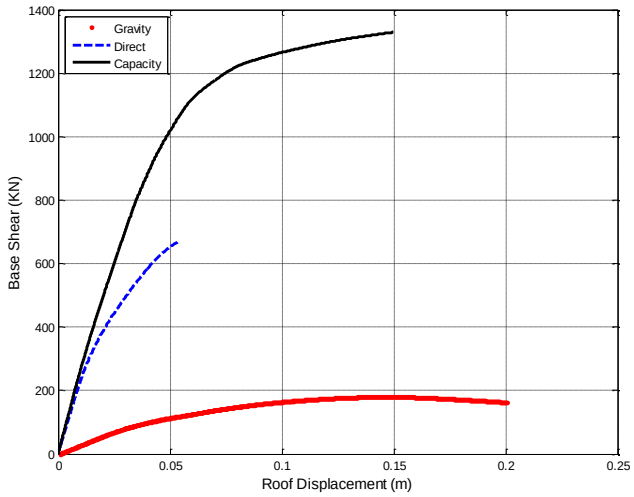

Fig. 13 Pushover curves of the three frame systems

5.2 Input ground motions

The input ground motion sequences selected in this study are divided into: (1) replicate motion sequences; and (2) random ground motion sequences. In replicate motion sequences, two identical ground motions are applied in series, with a sufficient time buffer to make sure that the structure is brought back to rest before applying the second record (Fig. 14), to investigate the effects of damage accumulation induced from the first earthquake on the behavior of the structure under the second earthquake while limiting ground motion parameters.

Three replicate sequences were selected based on different soil types and frequency contents. The first replicate sequence comprised of two identical records of the Loma Prieta earthquake applied in series. This record contains high frequency content and is measured on rock soil conditions. The second sequence used Chi-Chi earthquake record which is measured on soft soil conditions and contains low frequency content ground motions. A code compatible record, with a response spectrum that matches the ASCE-7 design spectrum is used in the third replicate sequence. The response spectra of the three records are shown in Fig. 15.

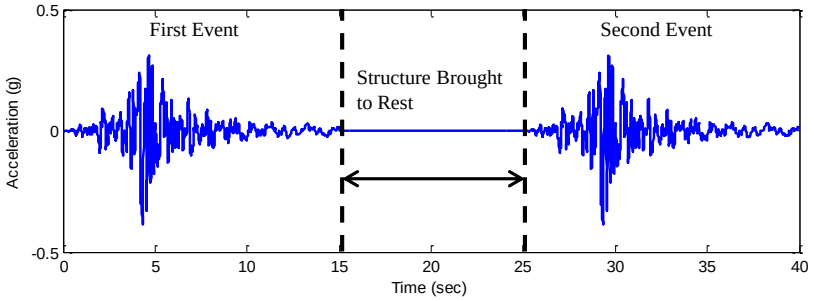

Fig. 14 Time buffer between two successive earthquakes to ensure that the structure is brought to rest; Loma Prieta earthquake recorded acceleration history

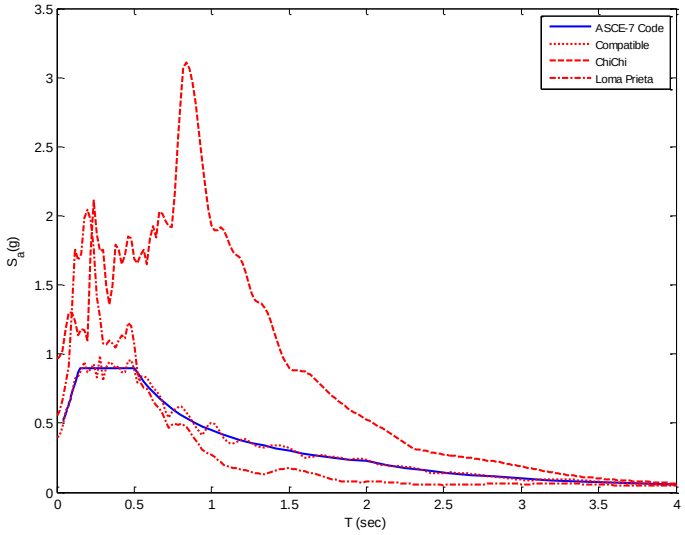

Fig. 15 Response spectra of the selected motions along with code design spectra

Table 5 Ground motion records

Record #	Earthquake	Station	Magnitude (M_w)	Distance (km)	Site condition
1	Loma Prieta	47379 Gilroy Array # 1	6.9	11.20	A
2	Victoria, Mexico	6604 Cerro Prieto	6.4	34.80	B
3	Imperial Valley	6605Delta	6.5	43.60	C
4	Kocaeli	Izmit	7.4	4.80	A
5	Whittier Narrows	90019 San Gabriel	6.0	9.00	A

Random earthquake sequences records are selected based on their frequency content and predominant periods. The ground motions in this case are applied in series with different sequence combinations. Three records are selected for each frame system, one of the three records has a predominant period so close to the first mode period of vibration of the structure; while the other two records have predominant periods much lower and higher than the frame first mode period of vibration. The predominant period of the ground motion defined by Miranda (1991) as the period at which the relative velocity of a linear system with 5% damping is maximum throughout the entire period range. The main advantage of using this approach is its simplicity and consistency to apply for a big number of earthquake ground motions.

For the gravity designed frame, records number 1, 2 and 3 (shown in Table 5) are selected. These records have 0.40, 1.12, and 1.58 sec. predominant periods respectively. Record 3 comprise the short period record where its predominant period is much lower than that the first fundamental period of the structure. The same selection criterion is used to select the ground motion records for the capacity designed frame. Records number 3, 4, and 5 are used for the analysis of the capacity designed frame. The ground motion parameters including magnitude, distance, and site conditions are shown in Table 5.

Nine earthquake sequences are applied to each of the gravity and capacity designed frame systems, since only two successive earthquake records are used in each sequence. Table 6 shows the earthquake sequences used for the gravity and capacity frames for the first and second applied records in series.

Individual records are scaled, for replicate and random earthquake sequences, to ensure constant demand to capacity (F/C) ratio for all three frame systems. The demand is chosen to be higher than or equal to the capacity, where the F/C ratio ranges between 1.0 and 2.75. The demand (F) is calculated as the spectral acceleration (S_a) from the elastic response spectra with 5% damping, at the first fundamental period of vibration multiplied by the weight of the structure (W). The capacity (C) is defined as the maximum base value (determined from the base shear versus displacement curve from the pushover analysis).

The F/C ratio is used for ground motion scaling to represent a wide range of ground motion shaking intensity from slight (F/C=1.00) to the severe case (F/C=2.75) of highly inelastic structural response. This scaling technique is used as an assumption to impose same level of ductility demand on the frame systems.

5.3 Response of degrading frame systems

The gravity frame is subjected to two identical Loma Prieta earthquake motions. Two scaling

Table 6 Earthquake sequences for gravity, direct, and capacity designed frame under two successive earthquake motions

	1st Record	2nd Record		1st Record	2nd Record
Gravity	1	1	**Capacity**	3	3
	1	2		3	4
	1	3		3	5
	2	1		4	3
	2	2		4	4
	2	3		4	5
	3	1		5	3
	3	2		5	4
	3	3		5	5

levels are considered using F/C ratios of 1.00 and 2.75. The purpose of having two distinct scaling levels is to investigate the effect of accelerations amplitude on the degrading response of the structure. Fig. 16 shows inter-story drift response histories of the first, second and third stories.

For F/C ratio equals to 1.00, the maximum inter-story drifts observed for the undamaged frame are 0.35%, 0.42%, and 0.84% for the first, second and third stories respectively. For the damage frame, the inter-story drifts are 0.38%, 0.44%, and 0.93%. The percentage increase in inter-story drifts in the damaged case is 8.57%, 4.79%, and 10.71% compared to the undamaged case. For F/C ratio equals to 2.75, inter-story drifts are 1.44%, 1.23%, and 2.16% for undamaged case and 2.00%, 1.67%, and 2.55% for damaged case; with a percentage increase of inter-story drifts in the damage case of 38.89%, 35.77%, and 18.06% for the first, second and third stories. It is worth noting that no plastic hinges were developed in the frame beam and column elements at F/C=1.00 for the damaged frame, while three plastic hinges were formed due to the second earthquake. In case of F/C=2.75, twenty four and twenty seven plastic hinges are developed for the undamaged and damaged cases respectively.

The results indicate that the ground motions amplitude for the replicate motion case has a significant impact on the response of the damaged model when compared to its undamaged counterpart. This is due to that when applying large acceleration amplitudes, larger forces are imposed on the system, and consequently higher inelasticity is introduced at the material level resulting in higher level of degradation.

In addition to studying the response of the gravity frame under replicate motions, the frame behavior under random motions is studied as well. Motions number 1 and 2 are used in this section. The sequences applied to the gravity frame are sequences 1-2 and 2-1. In sequence 1-2, record 1 is applied first to the frame system followed by record 2; while the opposite is true to sequence 2-1. Therefore, sequences 1-2 and 2-1 could be defined as reverse motion sequences.

Fig. 18 shows the inter-story drifts of the gravity designed frame under the two sequences, for F/C ratio equal to 2.00. In addition strain time histories monitored at reinforcing bars of sections located at both ends of column C2 are shown Fig. 19. For sequence 1-2, it is noted that the tensile strains did not reach twice the yield strain of the steel material during the whole sequence. On the other hand, in sequence 2-1, the strains were below the yield strain during record 2 however during record 1, the strains exceeded twice the steel yield strain.

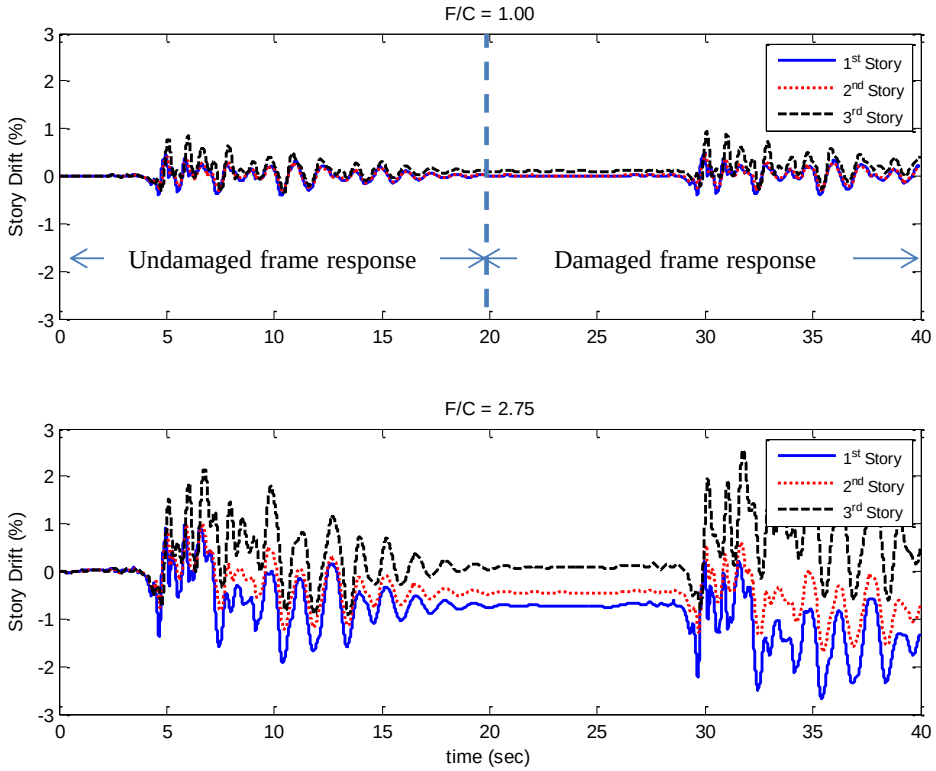

Fig. 16 Inter-story drifts under two identical Loma Prieta ground motions, F/C=1.00 (up) and 2.75 (down)

Table 7 provides a comparison between the response in terms of maximum inter-story drifts and number of developed plastic hinges monitored during the first and second records under sequences 1-2 and 2-1. The number of plastic hinges developed due to 1-2 and 2-1 sequences are 11 and 13 hinges; while for the first record only the, the number of developed hinges is 11 and 6. The discrepancies observed in the inter-story drifts and strains under reverse motion sequences indicate that the order of applied motions significantly affect the behavior of the frames.

The hysteresis loops of the first story for the gravity, direct, and capacity designed frames subjected to the replicate ground motion of the Loma Prieta earthquake record are shown in Fig. 17. The record is scaled to maintain an F/C ratio equal to 2.75. It is observed that from this plot that the amount of energy dissipation and absorption (area of the hysteretic curve) due to the first earthquake is more than the energy dissipated from the second earthquake. The reduction in the amount of energy absorbed during the second earthquake (when compared with the amount of energy absorbed due to the first earthquake) is more significant for the gravity and direct designed frame as opposed to the capacity designed frame.

5.4 Results and observations

The response of the three frames system is reported in terms of global and inter-story drifts and plastic hinges development. A comparison between the results of the gravity, direct (strength) and capacity designed frames is provided.

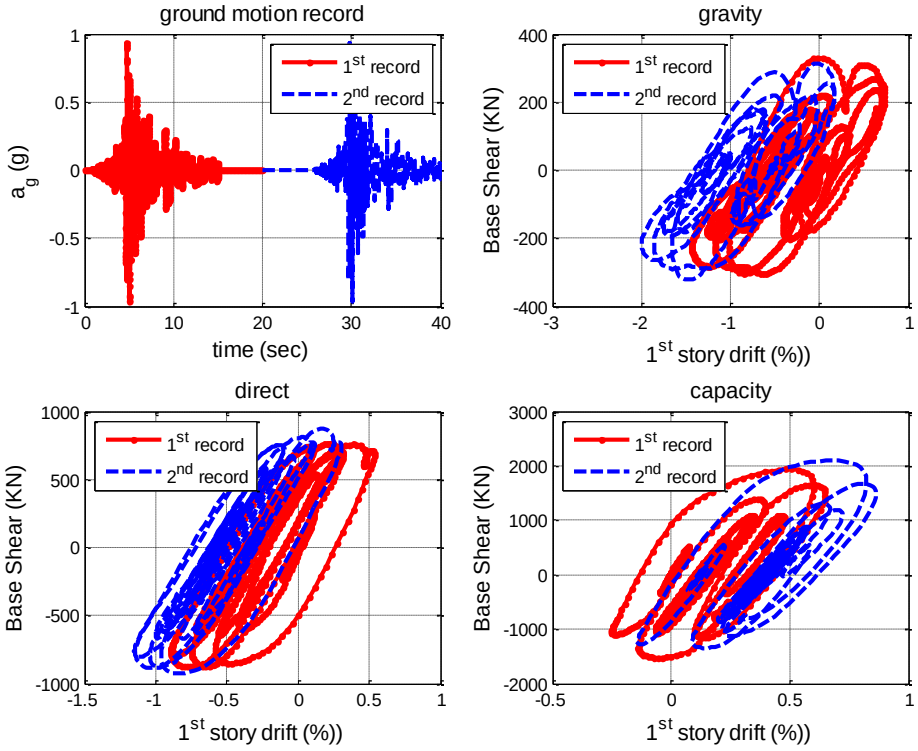

Fig. 17 Hysteretic loops of first story for the three frame systems subjected to the replicate motion of the Loma Prieta earthquake

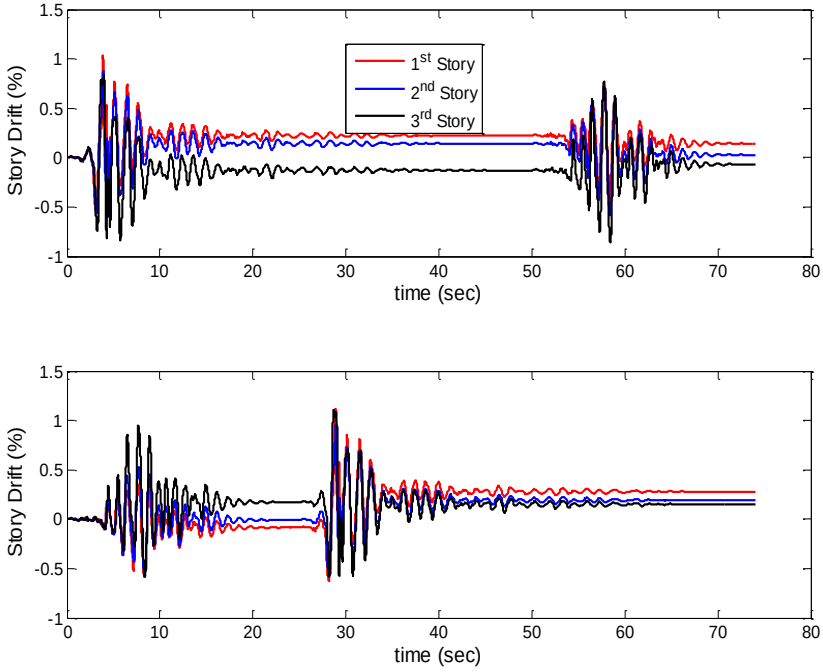

Fig. 18 Inter-story drifts under sequences 1-2 (up) and 2-1 (down)

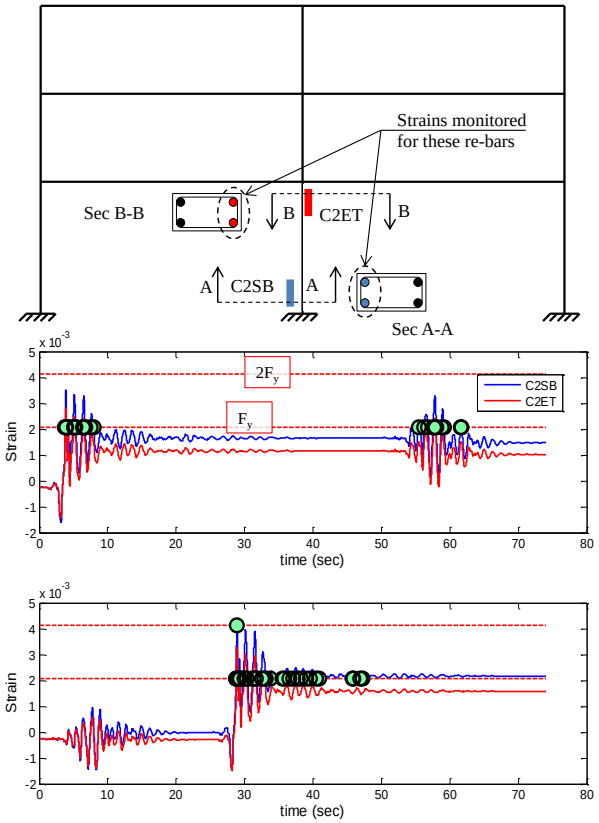

Fig. 19 Location of reinforcing bars where strains are monitored at (up), strains due to earthquake sequences 1-2 (middle) and 2-1 (down)

Fig. 20 and Fig. 21 show a comparison of the maximum total, first, second and third story drifts for all three frame systems due to the first and second records of the Chi-Chi and Loma Prieta replicate motion sequences, respectively. As shown in the figures, different scaling levels of F/C ratio are introduced. In the Chi-Chi sequence, the capacity designed frame experienced the largest drifts while the gravity designed frame experienced the least. In the Loma Prieta case, the opposite is observed since the gravity designed frame had highest drifts and capacity had the lowest.

It is worth noting that Chi-Chi earthquake record is measured on soft soil and had a long predominant period (1.2 sec) while the Loma Prieta record is of short period (0.3 sec) and is measured on rock. The fundamental periods of the gravity and capacity designed frames are 1.10 and 0.28 seconds. Therefore, it can be concluded that records of predominant periods closer to the structure first period of vibration impose lower demands on the system if the same F/C ratio is maintained. This is due to that the scaling procedure of ground motion records is based on equal spectral accelerations and hence smaller scaling factors are used for records of predominant period closer to frame fundamental period imposing smaller values of peak ground accelerations as well as spectral accelerations in a wider range of periods. However, this conclusion is only specific for this study and not a strict rule. This is also due to the fact that the frame under study may not be a single-mode dominated structure.

It is also observed that in Fig. 20 there is a significant increase in drifts in the second record for the capacity designed frame (especially in high F/C ratio) while in Fig. 21, the increase of drifts during the second record is more significant for the gravity designed frame.

Plastic hinges developed under the replicate code response spectrum compatible ground motion during the first and second earthquakes are provided in Fig. 22. The figure shows the number of plastic hinges formed with varying F/C ratio for the gravity, direct, and capacity designed frames. The maximum number of plastic hinges that could be developed in the frame systems is 60. As shown in Fig. 22, the capacity designed frame developed the maximum number of hinges. This is due to its ability to redistribute the strains from local regions of high inelasticity to regions of lower inelasticity during the earthquake sequences. Moreover, this indicates that capacity designed frames are better energy dissipative frames than their gravity and direct (strength) designed counterparts.

Table 7 Inter-story drifts and number of developed plastic hinges in the gravity designed frame during the 1st and 2nd records of earthquake sequences 1-2 and 2-1

		1-2		2-1	
		1st record	2nd record	1st record	2nd record
ID (%)	1st story	1.03	0.73	0.59	1.12
	2nd story	0.87	0.71	0.58	0.95
	3rd story	0.83	0.85	0.95	1.10
Number of Plastic hinges		11	11	6	13

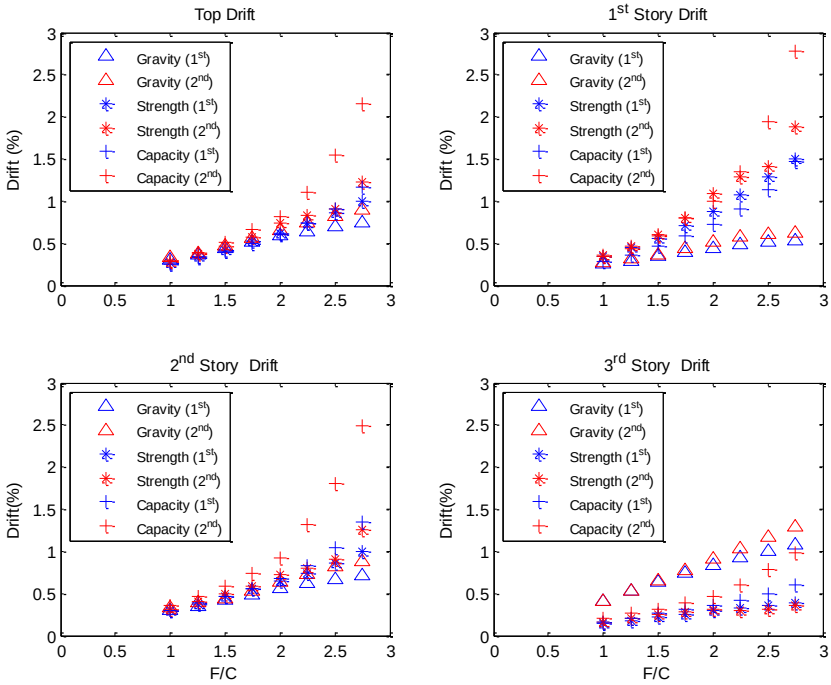

Fig. 20 Effect of F/C ratio on the maximum drifts during the first and second Chi-Chi earthquake replicate sequence

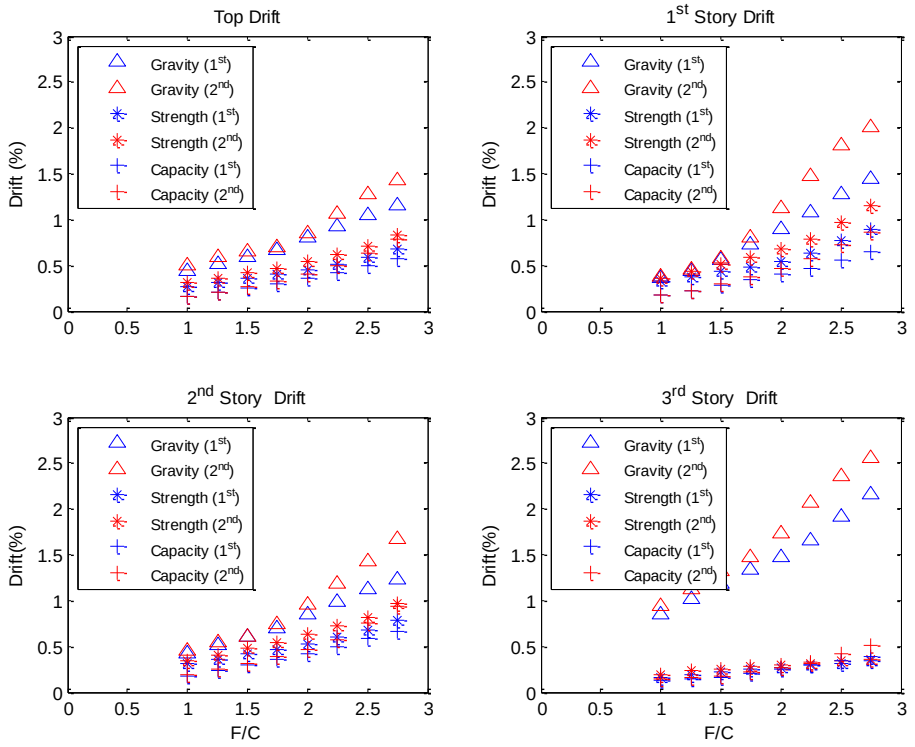

Fig. 21 Effect of F/C ratio on the maximum drifts during the first and second Loma Prieta earthquake replicate sequence

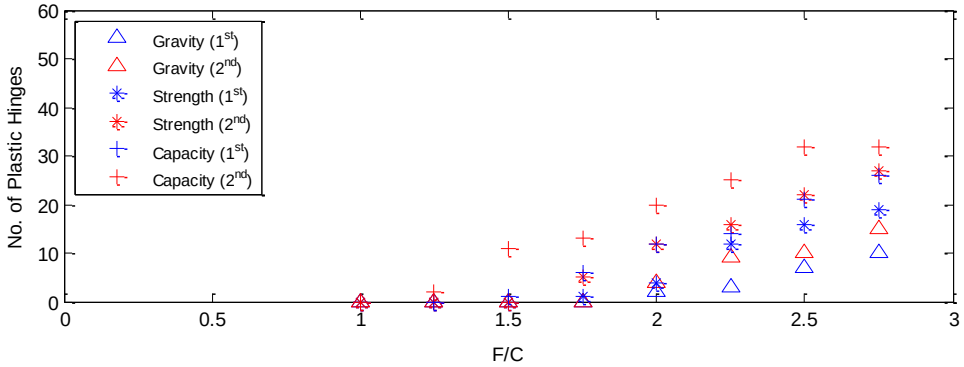

Fig. 22 Effect of F/C ratio on the number of plastic hinges developed in frames after applying the 1st and 2nd code compatible ground motions

Random earthquake sequences are applied to the gravity designed frame using different scaling levels of F/C ratio as shown in Fig. 23. The random sequences consist of 3 records that form 9 sequence combinations as shown in Table 6. For F/C equal to 1.00, the difference between maximum top drifts induced by the first and second records is negligible for all nine sequence combinations. This is due to that high inelasticity is not introduced to the frame system at F/C equal 1.00 and hence less degradation is induced. For F/C equal to 2.00 and 3.00 discrepancies

between the maximum drifts are observed for each earthquake sequence. Highest drift values are observed at motion sequences that contain records 1 and 3 (1-1, 1-3, 3-1, and 3-1). These two records are of predominant periods distinct to the frame fundamental period of vibration.

Fig. 24 shows the number of plastic hinges developed for the gravity and capacity designed frames under the random sequences of earthquake motions at F/C equal to 3.00. The capacity designed frame produced more plastic hinges during the earthquake sequences. In addition, plastic hinges recovery during the second earthquake is also observed for the capacity designed frame system since most of the capacity designed frame hinges are developed in beams and hence plastic hinges can recover easily in subsequent shaking. Plastic hinges recovery is observed in sequence 3-4 for the capacity frame.

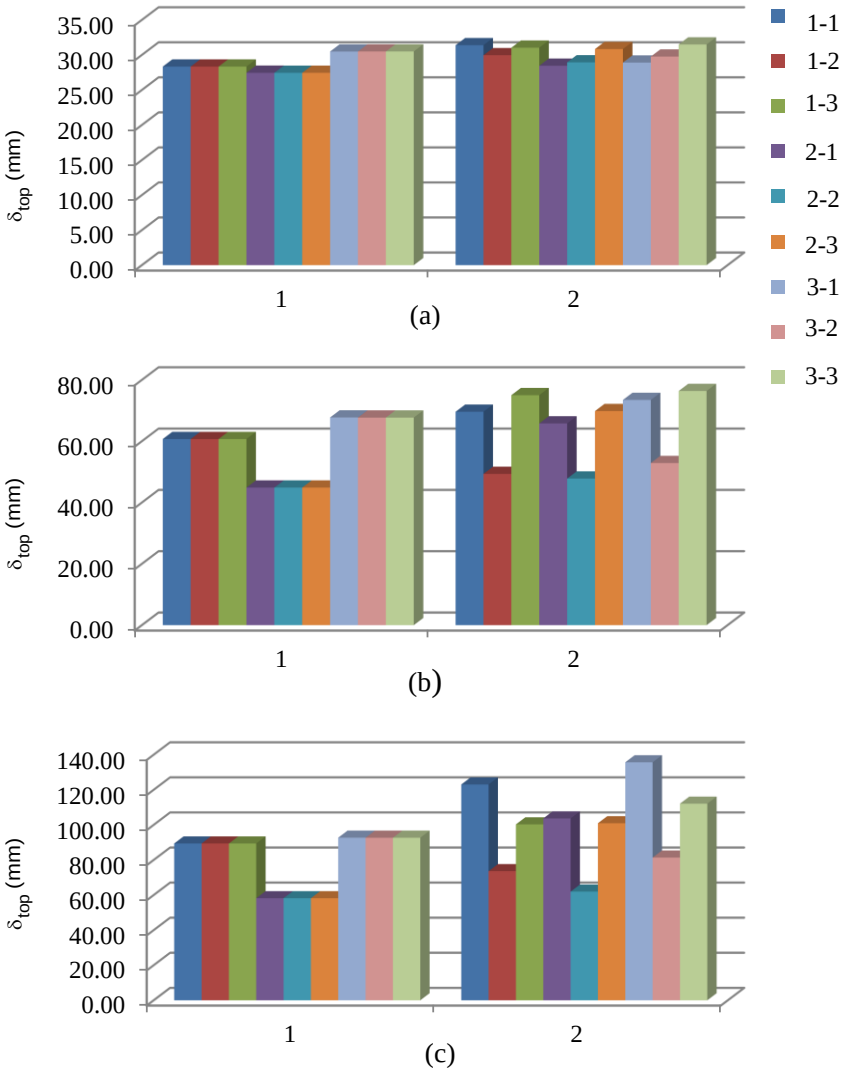

Fig. 23 Maximum top drifts of gravity designed frame, due to first (1) and second (2) motion, under random earthquake sequences; (a) F/C=1.00; (b) 2.00; (c) 3.00

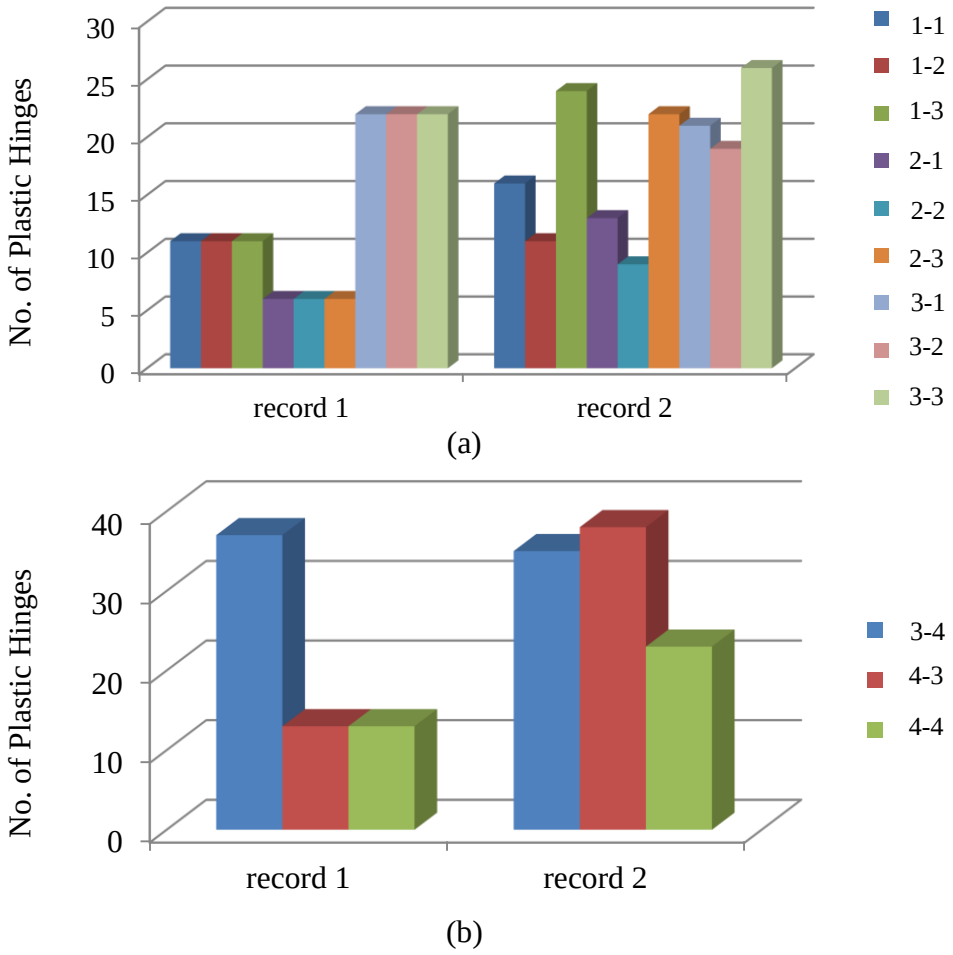

Fig. 24 Plastic hinges developed in the (a) gravity and (b) capacity designed frame systems

6. Conclusions

In this study, selected earthquake sequences area applied to three different types of RC frame systems. The earthquake sequences comprised a wide range of input motion parameters. The results shown in this paper indicate that multiple earthquakes can have a significant effect on the response of RC structural systems and hence the following conclusions are drawn:

- Multiple earthquakes have significant effect on the behavior of reinforced concrete structures in a manner that cannot be predicted from simple analysis.
- Damage induced to frame systems due to prior shaking affects significantly their performance under subsequent shaking.
- Capacity designed frames are proven to perform better than gravity and direct designed frames. The response of capacity designed frames under multiple earthquakes is characterized by formation of large number of plastic hinges and limited inter-story and global drifts. On the other hand, gravity and direct designed frames response showed unfavorable permanent deformations

and soft-story behavior, which was not the case for the capacity designed frame. This is due to that localized degradation was only introduced at capacity designed frame beams only, this allowed for force distribution in a ductile manner.

- The response of damaged and undamaged systems is compared using commonly used material models as well as steel and concrete models of degrading features. Based on the analysis results it is shown that multiple earthquake effects have significant impact on the behavior of reinforced concrete structures in a manner that cannot be predicted from simple analysis (conducted using commonly used models for design and assessment of reinforced concrete structures).

- This research confirms that the degrading response is not accurately captured based on simplified system level or component level models, that include damage features, presented in previous studies, this lead to reversing previous work recommendation.

References

Abdelnaby, A.E. (2012), "Multiple earthquake effects on degrading reinforced concrete structures", Ph.D. Dissertation, University of Illinois at Urbana-Champaign, IL, USA.

Amadio, C., Fragiacomo, M. and Rajgelj, S. (2003), "The effects of repeated earthquake ground motions on the non-linear response of SDOF systems", *J. Earthq. Eng.Struct. Dyn.*, **32**(2), 291-308.

American Society of Civil Engineers (ASCE 7-05) and Structural Engineering Institute (SEI) (2005), *Minimum design loads for buildings and other structures*, Reston, VA, American Society of Civil Engineers/Structural Engineering Institute.

Aschheim, M. and Black, E. (1999), "Effects of prior earthquake damage on response of simple stiffness-degrading structures", *J. Eng. Spectra*, **15**(1), 1-24.

Elnashai, A.S., Papanikolaou, V.K. and Lee, D. (2010), "ZEUS NL-a system for inelastic analysis of structures. User's manual", Mid-America Earthquake (MAE) Center, Department of Civil and Environmental Engineering, University of Illinois at Urbana-Champaign, Urbana.

Fragiacomo, M., Amadio, C. and Macorini, L. (2004), "Seismic response of steel frames under repeated earthquake ground motions", *J. Eng. Struct.*, **26**(13), 2021-2035.

Garcia, J. and Manriquez, J. (2011), "Evaluation of drift demands in existing steel frames as-recorded far-field and near-filed main shock-aftershock seismic sequences", *J. Eng. Struct.*, **33**, 621-634.

Ghosh, J., Padgett, J. and Sánchez-Silva, M. (2013), "Seismic damage accumulation of highway bridges in earthquake prone regions", *Earthq. Spectra*, **31**(1), 115-135.

Gomes, A. and Appleton, J. (1996), "Nonlinear cyclic stress-strain relationship of reinforcing bars including buckling", *J. Eng. Struct.*, **19**(10), 822-826.

Hancock, J. and Bommer, J.J. (2006), "A state-of-knowledge review of the influence of strong-motion duration on structural damage", *Earthq. Spectra*, **22**(3), 827-845.

Hatzigeorgious, G. (2010a), "Behavior factors for nonlinear structures subjected to multiple earthquakes", *Comput. Struct.*, **88**(5), 309-321.

Hatzigeorgious, G. and Beskos, D. (2009), "Inelastic displacement ratios for SDOF structures subjected to repeated earthquakes", *J. Eng. Struct.*, **31**(11), 2744-2755.

Hatzigeorgious, G. and Liolios, A. (2010b), "Nonlinear behavior of RC frames under repeated strong motions", *Soil Dyn. Earthq. Eng.*, **30**(10), 1010-1025.

Lee, J. and Fenves, G. (1998), "Plastic damage model for cyclic loading of concrete structures", *J. Eng. Mech.*, **124**(8), 892-900.

Li, Q. and Ellingwood, B. (2007), "Performance evaluation and damage assessment of steel frame buildings under main shock-aftershock earthquake sequences", *J. Earthq. Eng. Struct. Dyn.*, **36**(3), 405-427.

Mahin, S. (1980), "Effects of duration and aftershocks on inelastic design earthquakes", P*roceedings of the*

Seventh World Conference on Earthquake Engineering, Istanbul.
Mander, J.B., Priestley, M.J.N. and Park, R. (1988), "Theoretical stress-strain model for confined concrete", *J. Struct. Div*., *Am. Soc. Civ. Eng*., **114**(8), 1804-1826.
Menegotto, M. and Pinto, P.E. (1973), "Method of analysis for cyclically loaded reinforced concrete plane frames including changes in geometry and nonelastic behavior of elements under combined normal force and bending", *In Proceedings IABSE Symposium on Resistance and ultimate Deformability of Structures Acted on by Well-Defined Repeated Loads*, Lisbon.
Raghunandan, M., Liel, A., Ryu, H., Luco, N. and Uma, S. (2012), "Aftershock fragility curves and tagging assessments for a mainshock-damaged building", *15 WCEE*, Lisbon.
Ruiz-Garcia, J. (2010), "On the influence of strong-ground motion duration on residual displacement demands", *Earthq. Struct.*, **1**(4), 327-344.
American Society of Civil Engineers (ASCE 7-05) and Structural Engineering Institute (SEI) (2005), *Minimum design loads for buildings and other structures*, Reston, VA, American Society of Civil Engineers/Structural Engineering Institute.
ACI 318-08 (2008), "Building code requirements for reinforced concrete and commentary", American Concrete Institute, Detroit.
Miranda, E. (1991), "Seismic evaluation and upgrading of existing buildings", Ph.D. thesis, University of California at Berkley, Berkeley, California.

JL